Terrain Classification Based on Sensed Leg Compliance for Amphibious Crab Robot

John Grezmak, *Student Member, IEEE,* Nicole Graf, *Student Member, IEEE,* Alexander Behr, and Kathryn Daltorio, *Member, IEEE*

***Abstract*—Characterization of terrain in real time allows autonomous legged robots to modify their gait to better suit their environment and recognize hazardous conditions. We present a novel approach for terrain classification for legged robots with passively compliant components, in which terrain information is gathered by measuring component deflection during operation by means of low cost Hall effect magnetometers and embedded magnets. The effectiveness of this approach is demonstrated on a hexapod robot designed to operate in the surf zones of beaches. Datasets of sensor measurements corresponding to three types of granular terrain are collected in both a laboratory and outdoor beach environment, and are used to train support vector machine (SVM) classifiers. Results show that, using time domain features of measurements from each leg, a mean accuracy of 99.3% and 92.4% through 10-fold cross-validation can be achieved for the laboratory and beach datasets, respectively. For the beach dataset, this accuracy is found to be slightly greater than for a classifier trained on measurements from an on-board inertial measurement unit (IMU) (91.6%), while an accuracy of 95.1% can be achieved by combining the information from both sensor modalities as inputs to a single classifier. The effect of the Earth's magnetic field on the measurements and considerations for data collection are also discussed.**

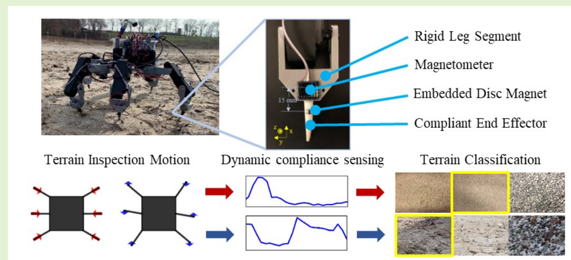

***Index Terms*—Legged robots, terrain classification, compliance sensing, support vector machine**

I. Introduction

TERRAINS consisting of granular media, such as soil, sand, rocks etc., can pose many challenges for legged robot locomotion. Granular terrains with different properties, such as volume fraction, can require the use of different gaits or control strategies to ensure efficient and safe locomotion [1]. Environments of this type are often encountered by amphibious robots, especially in the surf zones of beaches, where the properties of sandy or rocky terrain can vary depending on location and time of day. To enable autonomous locomotion of amphibious robots, it is critical for the robot to identify the terrain properties in real time and react appropriately.

The topic of autonomous terrain classification has received much attention in recent years, and has been investigated for a variety of robotic systems, including wheeled [2] and legged [3] robots. The problem typically consists of using one or more sensor modalities to gather information about the terrains the robot operates within, and training a classifier model in a supervised [4], [5], unsupervised [6], [7] or self-supervised [8] manner to predict a terrain label based on new measurements generated during operation. Several types of sensor modalities have been investigated for their use in terrain classification algorithms, with the choice often dependent on compatibility with the specific robotic system and the desired terrains to be differentiated (e.g. indoor versus outdoor terrains) [9].

For legged robots, both exteroceptive and proprioceptive sensors have been investigated for use in terrain classification algorithms. Exteroceptive sensors such as vision-based sensors [10] and IR-based depth sensors [11], [12] have been used for both indoor and outdoor terrain classification with legged robot systems. The drawbacks of methods relying on these sensors include the potential for poor real-world performance due to differences in terrain illumination and objects in the terrain not present in the samples used for model training [12]. For amphibious robots, turbid waters of surf zones also limit the applicability of exteroceptive sensors.

Several types of proprioceptive sensors have been investigated for legged robots including measurements of joint positions through encoders for both active [13], [14] and passive [5] joints, 6-axis force-torque (F/T) sensors [7], [9], [15], [16], and IMUs [5], [7]. Other proprioceptive sensors developed for particular legged robot designs include high resolution pressure sensor arrays [17], force sensing elements based on force sensitive resistors (FSRs) [4] and capacitive tactile sensing arrays [18]. Having multiple types of proprioceptive sensory inputs has also been shown to provide benefits over the use of single inputs for certain terrain types [5].

This research was partially funded by the Office of Naval Research under a Young Investigator Award (TTP19-0033) and by the Strategic Environmental Research and Development Program (SERDP) SEED Grant #MR19-1369 *(Corresponding author: Kathryn Daltorio)*

J. Grezmak, N. Graf, A. Behr and K. Daltorio are with the Department of Mechanical and Aerospace Engineering, Case Western Reserve University, Cleveland, OH, 44106 USA (email: jeg100@case.edu; nmg63@case.edu; amb296@case.edu; kathryn.daltorio@case.edu).

As proprioceptive sensors measure values internal to the robotic system, they rely on the robot actively interacting with the terrain. As a result, their measurements are affected by both the terrain type and the specific motion of the robot through the nonlinear dynamics of the robot-terrain interaction. The effect of stride frequency of legged robots on terrain classification ability through proprioceptive sensors was investigated in [19], [20]. Hoffman et al. [5] assessed the variability in measurements from proprioceptive sensors on a quadruped robot performing several gaits on a set of terrains, and concluded that, based on the large observed variability in feature distributions for different gaits, terrain classifiers should be preconditioned on a particular gait.

While the aforementioned studies have demonstrated good classification accuracy for their chosen set of terrains, few have included granular terrain in their experimental validation. Giguere et al. [21] investigated the use of inertial and actuator position sensors to determine whether a 6 degree of freedom (DOF) hexapod was traversing within or out of water in a beach environment. However, it is unknown how well this method can be extended to additional granular terrains or to robots with multiple DOFs per leg. Kolvenbach et al. [22] proposed an approach for classification of Mars-like granular terrains using F/T and IMU sensors mounted in a foot of a quadruped robot designed to perform an impact motion for gathering terrain information. Although results showed good classification accuracy with only IMU measurements, the method requires a foot design capable of impacting the terrain and producing measurable vibrations.

Because waterproofing of actuators and sensors is required for amphibious robots, many commonly used proprioceptive sensors, such as joint position encoders and F/T sensors, may be unavailable or require special design considerations [23]. Moreover, the need for particular end effector designs to optimize locomotion or perform specific tasks can prohibit the use of some contact-based sensors. To address these limitations, we present a terrain classification approach suitable for amphibious robots, in which a sensing system based on the application of low cost Hall effect magnetometers and magnets embedded in passively compliant components is proposed as a proprioceptive sensing modality for sensing robot-terrain interaction. This sensing system is easily waterproofed and is compatible with a variety of legged robot designs that exhibit some passive mechanical compliance in its limbs. Data collected by the sensors are used to train machine learning (ML) models to classify the underlying terrain type. We demonstrate this approach on an 18-DOF hexapod robot with compliant end effectors, which are utilized to implement the proposed sensing system. Two case studies are conducted to highlight the ability of the sensors to gather relevant terrain information through different open-loop motions, namely, a stationary probing motion and tripod gait. To our knowledge, this is the first demonstration of using Hall effect-based compliance sensors for gathering terrain information with legged robots.

The rest of this paper is organized as follows: Section II details the robotic system and the implementation of the compliance sensing system. In Section III, the details of the case studies are given, and the ML methods used to create the terrain classification models are detailed in Section IV. Results are presented and discussed in Section V, and conclusions are drawn in Section VI.

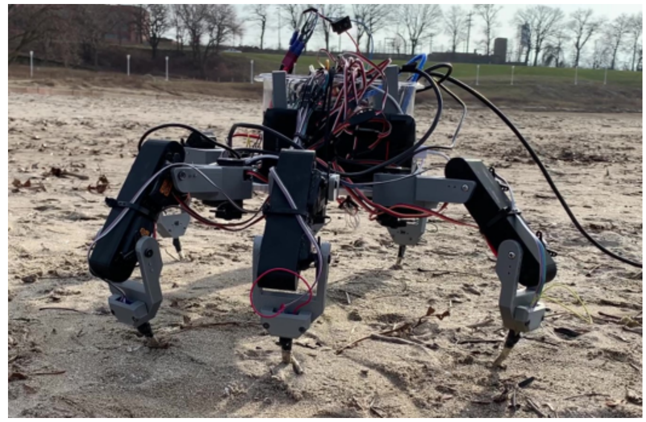

Fig. 1. Hexapod robot *Sebastian* operating in foreshore sand of beach environment.

II. Robot and Sensing System

A. Hexapod Robot System

A custom hexapod robot designed for amphibious operation, *Sebastian*, is chosen as the robotic system (Fig. 1). Each leg consists of four segments, with the three most proximal joints actuated by digital servomotors (Savox 1270TG) and the most distal segment a passively compliant end effector. The leg segment lengths have ratios inspired by biological crab anatomy, with the L1, L2 and L3 segments having lengths of 89.4 mm, 75.1 mm and 120.6 mm, respectively, as defined in Fig. 2. The end effector geometry is modeled after the distal segments of crab legs (i.e. dactyls), which has previously been shown to allow amphibious robots to better resist displacement from waves [24]. The leg segments and end effectors are fabricated using fused deposition modeling (FDM) with polylactic acid (PLA) and nylon (Taulman alloy 910, 55.8 MPa tensile strength, 502.9 MPa Young's modulus) materials, respectively. The robot uses on-board power sources and has a total weight of 4.63 kg.

The flexible nature of FDM fabricated nylon parts results in a passively compliant structure for the end effectors, which are attached to the final leg segment through a snap joint mechanism. Using FDM parameters of 100% infill and 0.2 mm layer height with PLA leg segment thickness of 12 mm, the resulting structure is effectively rigid in the leg segment while compliant in the end effector.

A Raspberry Pi 4 serves as an on-board CPU to communicate with an 18-pin Pololu Maestro servo controller and the sensing system described below.

B. Compliance Sensing System

Tactile sensors composed of Hall effect magnetometers and magnets embedded in compliant material have been demonstrated for robotic hands [25] and grippers [26]. Jamone et. al. [25] reported Hall effect-based tactile sensors employed on the fingers of a robotic hand could help realize a withdrawal reflex and classification of grasped objects. Chathuranga et al. [26] reported basic observations from an object manipulation task performed by a robotic gripper with soft hemispherical magnetic force sensors. However, the use of these sensors as feedback for walking robots has not been reported.

The passively compliant joint formed by the described end effector-leg segment connection is utilized to implement the Hall effect-based compliance sensors. A sensor mounted to one of these joints is shown in Fig. 2. A MLX90393 breakout board from Adafruit Industries, capable of three-axis magnetic field measurements up to 50 mT, is mounted near the end of the rigid leg segment. A grade N52 neodymium disc magnet (3/16 in. thickness and outer diameter), weighing 14.8% of the nylon end effector, is embedded in the end effector such that the desired dactyl-like profile is preserved. The magnet is held in place within the end effector with Gorilla Glue. Three-axis measurements from the sensors are collected at approximately 10 Hz with an Arduino Nano and sent to the on-board CPU.

Several factors are taken into account when choosing the location of the magnet in the end effector. Considering the measurement range of the magnetometer, the distance from the magnet to the magnetometer chip must be small enough to minimize measurement noise but large enough to prevent saturation. The distance to the joint bending axis affects the sensitivity of the sensor system (i.e. a distance further from the bending axis will result in larger relative movement of the magnetic field with respect to the magnetometer for a given applied force). A suitable horizontal distance between the embedded magnet and the magnetometer chip is empirically found to be 15 mm, based on the measured response of the sensors under loads expected to occur during normal operation.

Fig. 3 shows magnetometer measurements along the x-axis for loads of varying magnitude applied in the positive and negative z-axis directions at a distance of 24 mm from the end effector tip. The load range ($\pm$5 lb) is chosen to represent those encountered during normal operation. The measurements taken during loading (i.e. increasing the applied load) show an approximately linear response for both positive and negative loading directions. While some degree of hysteresis can be observed from the measurements taken during unloading, its effects on the ability of the sensing system to measure compliance under dynamic loads are considered negligible.

The MLX90393 has a resolution on the order of 0.1 μT, which is well below the magnitude of Earth's magnetic field ($\sim$60 μT). Measurements are therefore affected by both the orientation of the magnetometer with respect Earth's magnetic field and the relative position of the embedded magnet with respect to the magnetometer. As a result, dynamic measurements during operation will be affected by the robot's orientation, the motion of the legs with sensors and the end effector compliance due to terrain interaction. These aspects are explored in two case studies designed to highlight the ability to obtain terrain information through different leg motions.

III. Experimental Study

A. Open-loop Motion Generation

The two case studies investigate the use of different motions to generate terrain information through the interaction of the compliant limbs with the terrain. In generating these motions, we restrict the motion of end effector tips to follow straight paths at constant velocities with respect to the robot's frame of reference. The projection of a leg onto the robot's horizontal plane is given by:

$$s = L_1 + L_2 \cos\theta_2 + L_3 \cos(\theta_2 + \theta_3) \tag{1}$$

where s is the length of the projection, L_1, L_2 and L_3 are the segment lengths, and θ_1, θ_2 and θ_3 are the joint angles, as defined in Fig. 2. Similarly, the length of the projection onto the frontal plane is:

$$h = L_2 \sin\theta_2 + L_3 \sin(\theta_2 + \theta_3) \tag{2}$$

where h is the length of the projection. By taking the derivatives of the orthogonal components of s and of h, equations for the derivatives of the joint angles can be obtained as:

$$\dot{\theta}_1 = \frac{-v_x + \cos\theta_1[-L_2\dot{\theta}_2 \sin\theta_2 - L_3(\dot{\theta}_2 + \dot{\theta}_3)\sin(\theta_2 + \theta_3)]}{\sin\theta_1[L_1 + L_2\cos\theta_2 + L_3\cos(\theta_2 + \theta_3)]} \tag{3}$$

$$\dot{\theta}_2 = \frac{[v_y + v_x \cot\theta_1]\sin\theta_1 + L_3\dot{\theta}_3 \sin(\theta_2 + \theta_3)}{-L_2\sin\theta_2 - L_3\sin(\theta_2 + \theta_3)} \tag{4}$$

$$\dot{\theta}_3 = \frac{v_z - \dot{\theta}_2[L_2\cos\theta_2 + L_3\cos(\theta_2 + \theta_3)]}{L_3\cos(\theta_2 + \theta_3)} \tag{5}$$

where v_x, v_y and v_z are the velocities of the end effector tip in the x, y and z directions, respectively. Equations (3) - (5) form a system of equations that can be numerically integrated to result in a solution of joint angle positions over time that correspond to constant velocity end effector tip motion. To translate the joint angle solutions to robot motion, the solutions are down-sampled and stored as position commands to be sent sequentially to the servo controller.

B. Case Study I: Terrain Classification with Stationary Probing Motion

1) Motion Description: In this case study, a stationary probing motion utilizing each leg is used to gather terrain information. The robot starts in a standing position with legs oriented symmetrically about the frontal and sagittal planes. A set of legs forming a tripod are commanded to move with a horizontal inward motion of the foot tip of length 6 cm with a speed of 36 cm/s, where the direction of motion is towards the hip axis of rotation, as illustrated in Fig. 4. The foot tip is then raised to a position directly above its starting position with horizontal and vertical speeds of 36 cm/s and 18 cm/s, respectively, and finally returned to the starting position with a speed of 18 cm/s. These trajectories are then carried out for the set of legs forming the opposite tripod.

By performing this motion, several different terrain-end effector interactions take place. During stance, the end effectors penetrate the granular terrain to a depth dependent on its properties (i.e. volume fraction, friction, etc.). As the end effectors move inward during the initial phase of the trajectory, reaction forces from the terrain cause the compliant end effectors to deflect. It is expected that terrains with different properties produce different reaction forces (both in

This article has been accepted for publication in a future issue of this journal, but has not been fully edited. Content may change prior to final publication. Citation information: DOI 10.1109/JSEN.2021.3109864, IEEE Sensors Journal

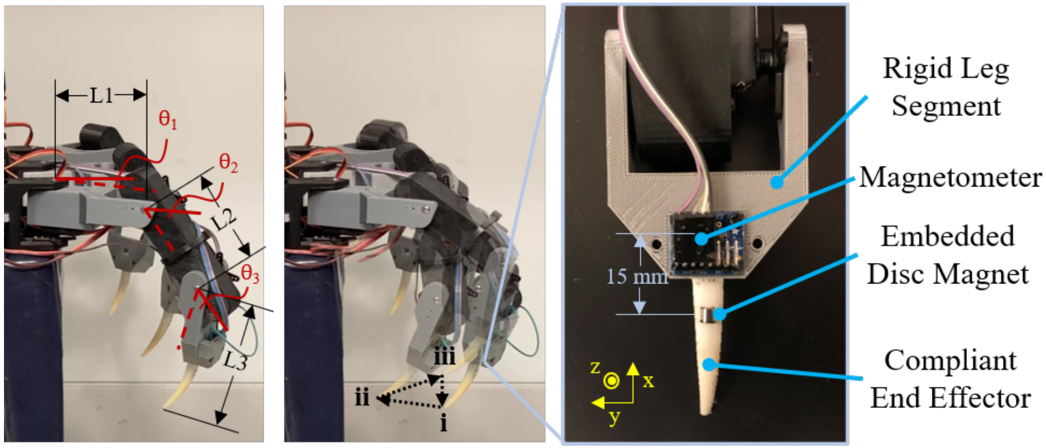

Fig. 2. (Left) Leg segment and joint angle definitions shown on right rear leg. (Middle) Trajectory of right rear leg end effector during the probing motion of case study I, shown as overlay of three positions: i) initial position, ii) position after pull inward, iii) position after raising from terrain. (Right) Hall effect magnetometer mounted on rigid robot leg segment above passively compliant end effector with embedded disc magnet.

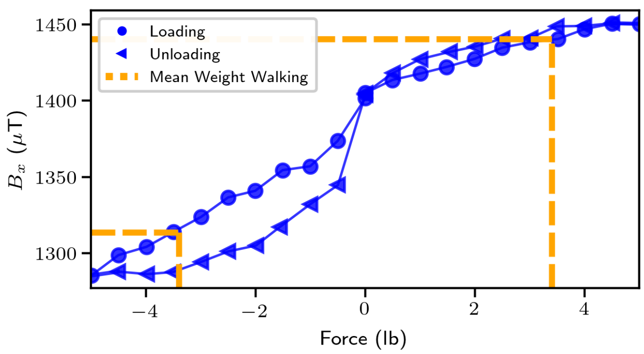

Fig. 3. Measured magnetic field along x-axis of the magnetometer of a Hall effect-based compliance sensor mounted on passively compliant joint subject to different applied loads. Loads corresponding to the mean weight forces during walking (one-third of robot's weight) are indicated by dashed lines.

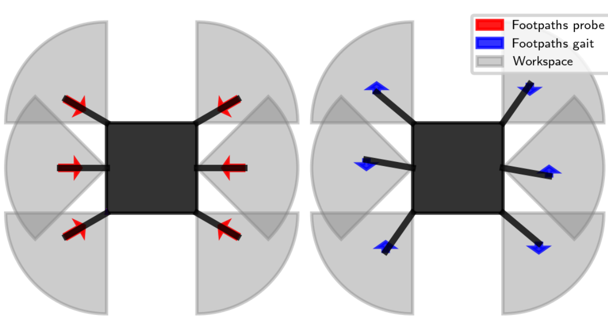

Fig. 4. Footpaths for case study I (left) and II (right) with projections of individual end effector workspaces illustrated.

magnitude and force distribution), thus producing different deflections of the end effectors as a function of time. As the legs are raised from the terrain, the robot's weight redistributes to the stationary tripod, which similarly can be expected to have terrain property-dependant effects on the end effector deflection. The final interaction takes place as the moving tripod returns to its initial position. Having each leg perform the motion provides a terrain inspection technique robust to local disturbances in the terrain.

2) Terrain Description: Three granular terrains representative of surf zones are prepared for this case study (Fig. 5). Pavestone natural play sand [1] is used to create two sand terrains with properties similar to those of the natural sand terrains used in case study II. With one terrain composed of the unaltered sand, referred to as dry sand, a second terrain is achieved by submerging the sand in water and allowing any water above the surface to evaporate. This second terrain is designed to be comparable to the compact sand in the foreshores of beaches, and is referred to hereafter as compact sand. Small rocks with average diameter of 2 cm are used as a third terrain. The terrains are prepared in containers large enough to allow the robot to stand in and complete the motion without interference.

3) Data collection: Data collected from each leg's sensor for one instance of performing the complete motion described is considered one trial. The terrain is switched out every five trials to minimize the effects of any potential drift in the sensor measurements or the robotic system (e.g. battery drain, servomotor damage, etc.). Trials of the robot performing the motion while suspended in air (i.e. "air walking") are also performed to serve as baseline measurements for which no terrain interaction occurs. For each trial, the robot is oriented in roughly the same direction with respect to Earth's magnetic field to control for its effects on the measurements. Measurements are collected for a total of 180 trials (45 per terrain including air walking).

C. Case Study II: Terrain Classification with Tripod Gait

1) Motion Description: In the second case study, we use a tripod gait to demonstrate gathering of terrain information while the robot is traversing the terrain. A gait cycle consisting of six phases is used with gait parameters chosen empirically

[1] https://www.homedepot.com/p/Pavestone-0-5-cu-ft-All-Purpose-Play-Sand-55141/100577543

Fig. 5. Granular terrains used for terrain classification with stationary probing motion; wet (compact) sand (left), dry sand (middle) and pebbles (right).

Fig. 6. Granular terrains of beach environment used for terrain classification with tripod gait; compact sand of foreshore (left), dry sand of backshore (middle) and small rocks/shells (right).

to produce stable gaits on each of the terrains used for data collection. A half-cycle starts with a tripod of legs lifting up and away from the body with horizontal and vertical foot tip speeds of 6 cm/s and 21 cm/s, respectively, to prevent the trailing leg from getting stuck due to the dactyl-like end effector profile. Both tripods then move together for a stride length of 27.3 cm with foot tip speed of 16.4 cm/s to push the robot forward, as illustrated in Fig. 4, with the swinging tripod also moving the foot tips horizontally back to their original distance from the body. The swinging tripod then plants down vertically with foot tip speed of 21 cm/s, and the motions then repeated for the opposite tripod to complete a gait cycle. Both tripods are in contact with the ground only during the 0.2s delay period after a tripod finishes its swing phase, corresponding to 9.1% of the gait cycle. With a delay of 0.2 s between each gait phase, the robot will have a maximum speed of approximately 2.5 cm/s under no-slip conditions.

Similar to the stationary probing motion, terrain property-dependant effects on the end effector deflection are expected to occur with weight redistribution during lifting or planting of the swinging tripod. However, in this case the end effectors are not dragged through the terrain as in the first phase of the probing motion, but experience reaction forces for the tripod in the stance phase as the robot is pushed forward. Due to the compliance of the end effector material, the end effector will still experience deflection in the direction of these reaction forces, albeit at a much smaller scale than for reaction forces perpendicular to the joint bending axis.

2) Terrain Description: The natural terrains of a beach environment (Edgewater Park, Cleveland, OH) are used for this case study (Fig. 6). During the time of data collection, sand in the foreshore and backshore beach areas were found to have different levels of compactness. The foreshore was therefore used as a source of a compact sand terrain and the backshore a dry sand terrain. An area of deposited small rocks and shells with diameters ranging from very small (3-5 mm) to approximately 20 mm was used as a third terrain source.

3) Data Collection: For one instance of data collection, again referred to as a trial, the robot is commanded to walk with the tripod gait for 25 steps. We collect 4 trials of the robot walking in each of the four cardinal directions for each terrain, to control for the effects of the Earth's magnetic field on the measurements. An on-board IMU recording angular velocity and linear acceleration in three directions is also used during the data collection.

IV. Machine Learning

A. Data Segmentation

For the first case study on probing motions, the measurements from one trial are used as a sample from which to predict the terrain type, resulting in a dataset of 180 samples. For the second case study, the measurements from each trial (i.e. 25 steps) are segmented into 23 samples discarding the first and last steps, each of which are used to independently predict the terrain type. This results in a dataset 1192 samples. The datasets for each case study are treated independently for the purpose of ML.

B. Feature Extraction

The magnetometer measurements consist of three-axis (with respect to sensor, as defined in Fig. 2) magnetic field measurements from each leg of the robot, for a total of 18 signals. The on-board IMU used for the second case study accounts for an additional 6 signals. To reduce the dimensionality of these signals, we extract time domain features to obtain feature vectors, which are used as the inputs to classifiers.

During data collection in the beach environment, it was unexpectedly found that ferrous material in the backshore sand would attach to the magnets during operation, causing an effect resembling an offset in the magnetometer measurements. As the amount of attached material could vary between trials and even steps within a trial, the offset effect is difficult to model or adjust for. To prevent performance issues in ML models trained on this data, we avoid using features such as the first moment of the data and the magnitude of specific data points, and instead use features related to the distribution or "shape" of the data points within a sample.

Six feature types were chosen on the basis of having minimal drift among the samples from the dry sand trials: 1) range, 2) standard deviation (second moment), 3) skewness (third moment), 4) kurtosis (fourth moment), 5) shape factor (root mean square (RMS) divided by mean of absolute value), and 6) crest factor (peak value divided by RMS). These feature types are used for feature extraction for both case studies.

For the first case study, the probing motion caused minimal changes to measurements along the y- and z- axes compared to the x-axis. For this reason, only the x-axis data are used for feature extraction in this case study. Feature extraction using the six chosen feature types results in a feature vector of size 36 when using measurements from the sensors of each leg.

For the second case study, magnetometer measurements from each axis are used for feature extraction, resulting in 108 features. Feature extraction from the IMU measurements provides an additional 36 features. Because walking direction is another known variable for each trial, an additional feature corresponding to walking direction can be included. We train classifiers using each possible combination of sensor modalities (e.g. magnetometer data only, IMU data only, and both) with and without the use of direction as a feature.

C. Classification Model

A one-versus-one SVM is chosen as the ML model for classifying terrain from the feature vectors. SVMs are a popular choice for terrain classification as they are often found to have superior performance compared to other ML methods and have been used with various types of proprioceptive sensors [5], [27]. SVMs also provide good robustness to overfitting even in cases of training on small datasets with relatively large feature vector sizes [13]. We use a radial basis function (RBF) kernel for the SVM classifier; while it is unknown what the optimal kernel choice for this dataset is, the RBF kernel was found to outperform linear kernels or other standard kernels (e.g. polynomial) for the many different models trained and tested. 10-fold cross validation is used to evaluate the classifier performance in terms of mean classifier accuracy.

V. Results and Discussion

A. Terrain Discrimination from Compliance Sensing

1) Case Study I: The average measurements from the right-rear leg during each trial of the probing motion in each terrain type and while suspended in air are shown in Fig. 7. At time $t = 0$, the leg begins the motion by pulling the foot tip inwards through the terrain. The effects of the ground reactions forces on the end effector deflection can be seen by the increase in the magnetic field values measured by the magnetometer. This is opposed to the case of the robot suspended in air, which shows relatively constant measurements during this time period. At approximately $t = 0.36$ when the leg is lifted from the terrain, the measurements from each terrain type can be seen to converge to a value similar to that from air walking. As the legs are then planted beginning at approximately $t = 0.72$, terrain dependent effects can be seen in the measurements as the robot's weight is redistributed amongst the legs before the opposite tripod begins to move.

Principal component analysis (PCA) is applied to the feature vectors of the corresponding dataset, and the projection of the first two principal components are shown in Fig. 8. Clusters corresponding to each terrain type can be seen with noticeable separation along these projections. Dry and compact sand samples have relatively tight clusters close in proximity, while the pebbles samples have a more dispersive yet still mostly separate cluster. The larger dispersion of the pebbles samples is likely a result of the large pebble size with respect to the end effectors, which can lead to larger trial-to-trial variance in the local terrain geometry when the robot is placed in the terrain and thus the resulting robot-terrain interaction. The air walking samples have the tightest cluster, which is highly separated from the rest of the data along the first principal component axis. These observations of the data's structure in the projected space make intuitive sense and suggest the magnetometers have collected terrain-relevant information during the probing motion.

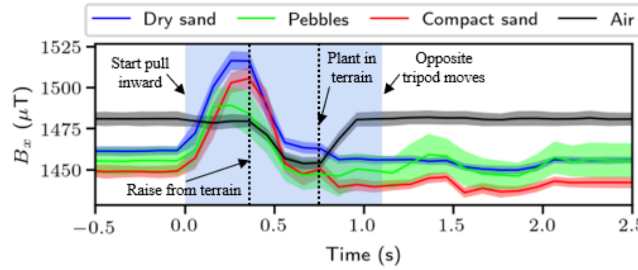

Fig. 7. Average x-axis measurements from magnetometer on the right-rear leg over all trials of probing motion performed in each terrain (case study I), shown with shaded error bars. The time period during which the leg is in motion is highlighted in blue.

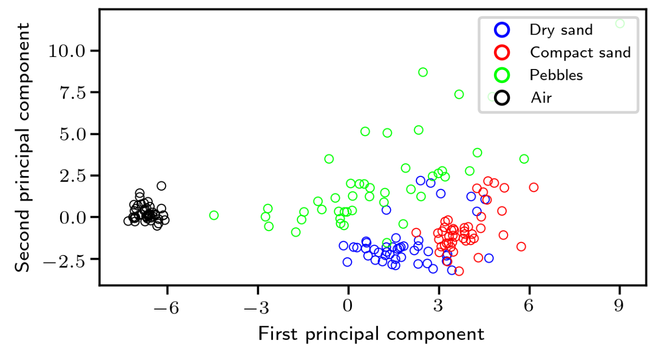

Fig. 8. First two principal components of the feature vectors from the dataset of case study I.

2) Case Study II: Measurements from the middle-left leg for 10 seconds of walking in the east direction for a trial from each terrain type are shown in Fig. 9. The measurements are adjusted to counter the offset effects from the ferrous material during data collection.

As the middle-left leg starts in the stance phase during a gait cycle, the first change in ground reaction forces occurs when the opposite tripod lifts from the terrain. The effects of this can be seen by the initial dip in x-axis measurement values during the beginning of the first step. This dip can be seen to be largest for the compact sand terrain while being comparable for the compact sand and rocks/shells terrains. This aligns with observations of the end effector penetration into the terrains during operation; for the compact sand, the penetration was on average much less than for dry sand and rocks/shells, which tended cause full penetration into the terrain. The measurements become comparable as the leg begins the swing phase of the gait cycle at $t = 1.1$, with slight differences seen at the end of the gait cycle when the leg plants down.

The projection of the first two principal components of the dataset of feature vectors from both sensor modalities are shown in Fig. 10. Clear separation between classes as clusters could not be seen in a similar plot for feature vectors of only the magnetometer data, but can be seen for the combined features. Each value is plotted indicating its corresponding terrain by color and walking direction by marker. No extensive clustering of samples based on direction can be seen, suggesting the features have robustness to the direction of walking.

This article has been accepted for publication in a future issue of this journal, but has not been fully edited. Content may change prior to final publication. Citation information: DOI 10.1109/JSEN.2021.3109864, IEEE Sensors Journal

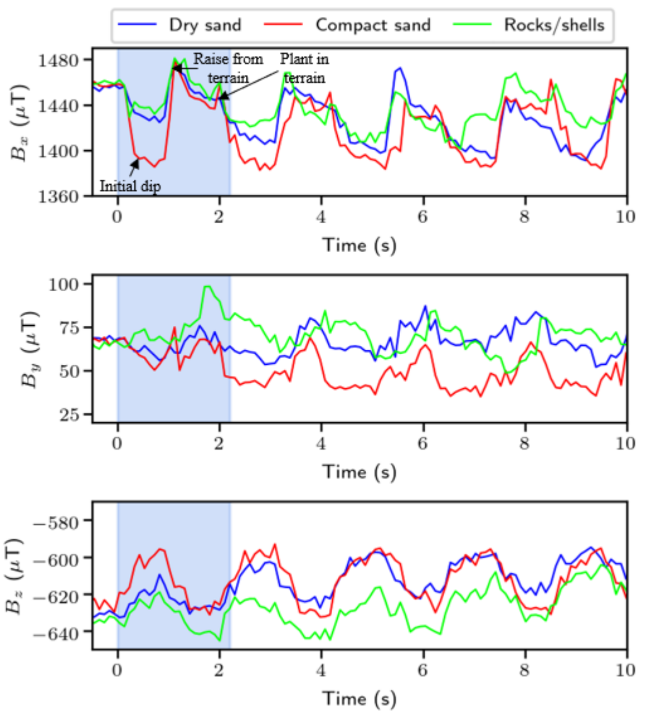

Fig. 9. 3-axis measurements from magnetometer on the middle-left leg for 10 seconds of walking in each terrain. The time period for the first complete gait cycle is highlighted in blue.

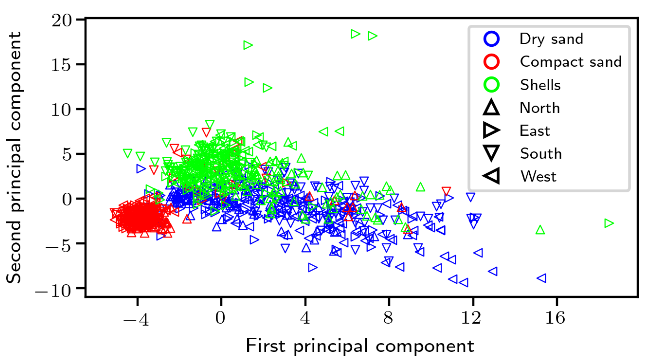

Fig. 10. First two principal components for feature vectors from dataset using both sensor modalities of case study II.

A similar distribution of terrain-related clusters in this space to that of the dataset for case study I can be seen, although the dry sand cluster exhibits much more dispersion for this dataset. This is likely due to the non-uniformity of the natural terrain causing more variability in the data generation process.

B. Classification Results

1) Case Study I: SVMs trained on datasets with and without including the air walking samples achieve a mean accuracy of 98.4% and 99.3%, respectively. The lower classification accuracy for the former was found to be a result of misclassification of some pebbles samples as being air walking samples. While in the pebbles terrain, the robot would on occasion be only supported by a subset of its legs, with little terrain interaction

TABLE I
TESTING ACCURACY FOR DIFFERENT COMBINATIONS OF FEATURES.

Sensor modalities	Mag. only	IMU only	Mag. + IMU
Without direction	91.34%	91.22%	94.77%
With direction	92.43%	91.58%	95.12%

TABLE II
TESTING ACCURACY ON DATA FROM DIRECTIONS HELD OUT.

Direction	North	East	South	West
Cross validation	96.6%	95.2%	95.7%	94.0%
Testing accuracy	74.3%	93.5%	85.7%	93.1%

occurring for the rest of the legs. This would result in the measurements for those legs resembling those for air walking. The overall high classification accuracy under the controlled conditions of this case study provide confidence for extending the method to less structured real world environments.

2) Case Study II: The mean accuracies of SVMs trained on each combination features are listed in Table I. Without including walking direction as a feature, SVMs trained on only the magnetometer data or the IMU data perform comparably. The inclusion of walking direction for the IMU data has little effect on the classification accuracy (i.e. 0.3% increase), but improves classification accuracy for the magnetometer data by over 1%. The combination of the sensor modalities results in higher classification accuracy than either alone, the highest occurring when including walking direction as a feature.

C. Data Collection Considerations

The ability to correctly classify terrain from data of a walking direction not present during training is also investigated. Specifically, SVMs are trained on datasets of each possible combination of three walking directions, with the data from the remaining directions used for testing. Using features from both sensor modalities based on previous results, the resulting testing accuracies, along with results of 10-fold cross validation on the training datasets, are listed in Table II. For the cases where the east or west direction data are held out, the cross validation result and accuracy on the held out data are comparable. However, for the cases where north or south data are held out, the accuracy on the held out data is much lower. The confusion matrices for the classification on the held out data are shown in Fig. 9, which reveal misclassification of dry sand and rocks/shells samples for the north and south data. This may be a result of the high variability within these terrains causing similar measurements for some trials. Still, these results suggest that by using features capturing the shape of the samples rather than their magnitudes, robust classifiers can still be trained on data from limited walking directions.

VI. CONCLUSIONS AND DISCUSSION

We demonstrate a novel use of Hall effect-based compliance sensing for gathering terrain information with a legged robot. With the sensing system applied to the compliant end effectors of a hexapod robot, two case studies are performed which

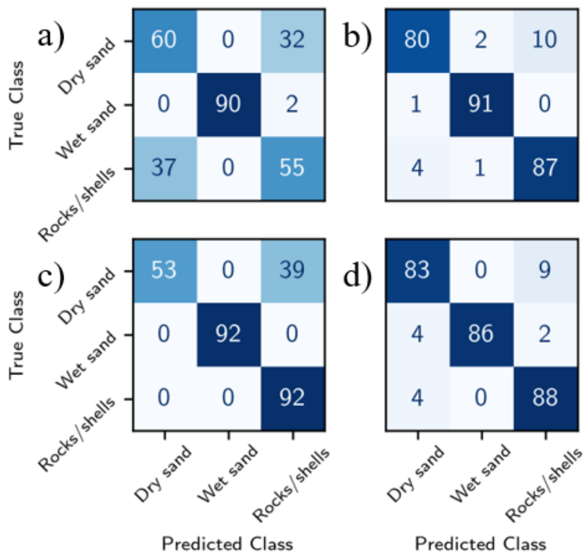

Fig. 11. Confusion matrices for prediction results on data of directions held out: a) north b) east c) south d) west.

demonstrate the use of different motions (probing motion during stance or walking) for gathering terrain information with the sensors. We show that good classification results using SVM classifiers can be achieved for both datasets. The compliance sensing can be used instead of or to complement IMU measurements for terrain classification during walking.

We expect this to be particularly valuable for amphibious locomotion, where different strategies may be appropriate for different terrains. These sensors are low cost and easily waterproofed, which can make them feasible to implement on robots with many DOF or robot swarms with many individuals. In particular, an advantage is that no electrical connection is required between the transducer and the compliant dactyl where the critical deformation occurs.

We show that the Earth's magnetic field does not preclude the use of these sensors when the robot's orientation changes with respect to it, suggesting future robots may be able to take advantage of this type of sensor information in various tasks (e.g. gait adaptation, identification of environmental hazards, or path planning near changing water lines.)

While this paper focused on sensed compliance in the distal segment of each of six legs, many other configurations are possible. Using fewer sensors may enable similarly robust classification but with more training data. Additional compliance in the dactyl to amplify deformation may enable faster classification, for example within a single step. The use of this approach in practical applications may be enhanced through investigation of the performance of ML models trained on data collected under controlled conditions (such as in case study I) to predict terrains in real-world settings (such as in case study II).

Acknowledgment

This research was partially funded by the Office of Naval Research under a Young Investigator Award (TTP19-0033) and by the Strategic Environmental Research and Development Program (SERDP) SEED Grant #MR19-1369. The authors would like to thank Yifeng Gong for assistance with data collection, Prof. Jennifer Taylor for insights into crab behavior in surf zones, Lauren Ficek, Quinn Foley and Clay Inman for preliminary designs of compliance sensors, and Joseph Richmond for preliminary design of *Sebastian* robot.

References

[1] C. Li, P. B. Umbanhowar, H. Komsuoglu, D. E. Koditschek, and D. I. Goldman, "Sensitive dependence of the motion of a legged robot on granular media," *Proc. Nat. Acad. Sci.*, vol. 106, no. 9, pp. 3029–3034, 2009.

[2] M. Mei, J. Chang, Y. Li, Z. Li, X. Li, and W. Lv, "Comparative study of different methods in vibration-based terrain classification for wheeled robots with shock absorbers," *Sensors*, vol. 19, no. 5, pp. 1–18, 2019.

[3] C. Kertész, "Rigidity-based surface recognition for a domestic legged robot," *IEEE Robot. Autom. Lett.*, vol. 1, no. 1, pp. 309–315, 2016.

[4] M. A. Hoepflinger, C. D. Remy, M. Hutter, L. Spinello, and R. Siegwart, "Haptic terrain classification for legged robots," in *Proc. Int. Conf. Robot. Automat. (ICRA)*, 2010, pp. 2828–2833.

[5] M. Hoffmann, K. Štěpánová, and M. Reinstein, "The effect of motor action and different sensory modalities on terrain classification in a quadruped robot running with multiple gaits," *Robot. Auton. Syst.*, vol. 62, no. 12, pp. 1790–1798, 2014.

[6] P. Giguere and G. Dudek, "Clustering sensor data for autonomous terrain identification using time-dependency," *Auton. Robot.*, vol. 26, pp. 171–186, 2009.

[7] P. Dallaire, K. Walas, P. Giguère, and B. Chaib-draa, "Learning terrain types with the Pitman-Yor process mixtures of Gaussians for a legged robot," in *Proc. Int. Conf. Intell. Robot. Syst. (IROS)*, 2015, pp. 3457–3463.

[8] W. Shi, Z. Li, W. Lv, Y. Wu, J. Chang, and X. Li, "Laplacian support vector machine for vibration-based robotic terrain classification," *Electron.*, vol. 9, no. 3, 2020.

[9] K. Walas, "Terrain classification and negotiation with a walking robot," *J. Intell. Robot. Syst.*, vol. 78, pp. 401–423, 2015.

[10] S. Zenker, E. E. Aksoy, D. Goldschmidt, F. Wörgötter, and P. Manoonpong, "Visual terrain classification for selecting energy efficient gaits of a hexapod robot," in *Proc. Int. Conf. Adv. Intell. Mechatron.*, 2013, pp. 577–584.

[11] T. Homberger, M. Bjelonic, N. Kottege, and P. V. K. Borges, "Terrain-dependant control of hexapod robots using vision," in *Proc. Int. Symp. Exp. Robot.*, 2017, pp. 92–102.

[12] Y. Zhu, C. Jia, C. Ma, and Q. Liu, "SURF-BRISK–based image infilling method for terrain classification of a legged robot," *Appl. Sci.*, vol. 9, no. 9, 2019.

[13] G. Best, P. Moghadam, N. Kottege, and L. Kleeman, "Terrain classification using a hexapod robot," in *Proc. Australasian Conf. Robot. Automat.*, 2013, pp. 1–8.

[14] J. Mrva and J. Faigl, "Feature extraction for terrain classification with crawling robots," in *Info. Technol. - Appl. Theory*, vol. 1422, 2015, pp. 179–185.

[15] J. Bednarek, M. Bednarek, L. Wellhausen, M. Hutter, and K. Walas, "What am i touching? Learning to classify terrain via haptic sensing," in *Proc. Int. Conf. Robot. Automat. (ICRA)*, 2019, pp. 7187–7193.

[16] L. Wellhausen, A. Dosovitskiy, R. Ranftl, K. Walas, C. Cadena, and M. Hutter, "Where should i walk? Predicting terrain properties from images via self-supervised learning," *IEEE Robot. Autom. Lett.*, vol. 4, no. 2, pp. 1509–1516, 2019.

[17] J. J. Shill, E. G. Collins, E. Coyle, and J. Clark, "Terrain identification on a one-legged hopping robot using high-resolution pressure images," in *Proc. Int. Conf. Robot. Automat. (ICRA)*, 2014, pp. 4723–4728.

[18] X. A. Wu, T. M. Huh, R. Mukherjee, and M. Cutkosky, "Integrated ground reaction force sensing and terrain classification for small legged robots," *IEEE Robot. Autom. Lett.*, vol. 1, no. 2, pp. 1125–1132, 2016.

[19] F. L. Garcia Bermudez, R. C. Julian, D. W. Haldane, P. Abbeel, and R. S. Fearing, "Performance analysis and terrain classification for a legged robot over rough terrain," in *Proc. Int. Conf. Intell. Robot. Syst.*, 2012, pp. 513–519.

[20] S. Manjanna, G. Dudek, and P. Giguere, "Using gait change for terrain sensing by robots," in *Proc. Int. Conf. Comput. Robot Vision*, 2013, pp. 16–22.

[21] P. Giguère, G. Dudek, S. Saunderson, and C. Prahacs, "Environment identification for a running robot using inertial and actuator cues," in *Robot.: Sci. Syst. II*, 2006.
[22] H. Kolvenbach, C. Bärtschi, L. Wellhausen, R. Grandia, and M. Hutter, "Haptic inspection of planetary soils with legged robots," *IEEE Robot. Autom. Lett.*, vol. 4, no. 2, pp. 1626–1632, 2019.
[23] A. Khan, W. Liquan, W. Gang, M. Imran, H. M. Waqas, and A. A. Zaidi, "Concept design of the underwater manned seabed walking robot," *J. Mar. Sci. Eng.*, vol. 7, no. 10, 2019.
[24] N. Graf, A. Behr, and K. A. Daltorio, "Dactyls and inward gripping stance for amphibious crab-like robots on sand," *Bioinspiration and Biomimetics*, 2021.
[25] L. Jamone, L. Natale, G. Metta, and G. Sandini, "Highly sensitive soft tactile sensors for an anthropomorphic robotic hand," *IEEE Sensors J.*, vol. 15, no. 8, pp. 4226–4233, 2015.
[26] D. S. Chathuranga, Z. Wang, Y. Noh, T. Nanayakkara, and S. Hirai, "A soft three axis force sensor useful for robot grippers," in *Proc. Int. Conf. Intell. Robot. Syst. (IROS)*, 2016, pp. 5556–5563.
[27] C. Weiss, N. Fechner, M. Stark, and A. Zell, "Comparison of different approaches to vibration-based terrain classification," in *Proc. 3rd European Conf. Mobile Robot.*, 2007, pp. 1–6.